

Spatial and temporal variability of $p\text{CO}_2$ and CO_2 emissions from the Dongjiang River in South China

Boyi Liu¹, Mingyang Tian², Kaimin Shih³, Chun Ngai Chan¹, Xiankun Yang⁴, Lishan Ran¹

5 ¹Department of Geography, the University of Hong Kong, Hong Kong SAR, China

²Institute for Geology, Center for Earth System Research and Sustainability (CEN), Universität Hamburg, Hamburg, Germany

³Department of Civil Engineering, the University of Hong Kong, Hong Kong SAR, China

⁴School of Geographical Sciences, Guangzhou University, Guangzhou, 510006, China

10

Correspondence to: Lishan Ran (lsran@hku.hk)

Abstract. CO_2 efflux at the water–air interface is an essential component of the riverine carbon cycle. However, the lack of spatially resolved CO_2 emission measurement still hinders the accuracy of estimates on global riverine CO_2 emissions. By deploying floating chambers, seasonal changes in river water CO_2 partial pressure ($p\text{CO}_2$) and CO_2 evasion from the Dongjiang River in South China were investigated.

15

~~Spatial and temporal patterns of $p\text{CO}_2$. Lateral soil CO_2 input and dilution effect caused by precipitation played critical roles in controlling riverine $p\text{CO}_2$ in small rivers, while the decomposition of allochthonous organic carbon is responsible for $p\text{CO}_2$ variability in large rivers. were mainly affected by terrestrial carbon inputs and in-stream metabolism, both of which varied due to differential catchment settings, land cover, and hydrological conditions.~~ Temperature-normalized gas transfer velocity (k_{600}) in

20

small rivers were $8.29 \pm 11.29 \text{ m d}^{-1}$ and $4.90 \pm 3.82 \text{ m d}^{-1}$ for the wet season and dry season, respectively, which were nearly 70 % higher than that of large rivers ($3.90 \pm 5.55 \text{ m d}^{-1}$ during the wet season and $2.25 \pm 1.61 \text{ m d}^{-1}$ during the dry season). A significant correlation was observed between k_{600} and flow velocity but not wind speed regardless of river size. Majority of the surveyed rivers were net CO_2 source,

25

~~while~~ exhibiting substantial seasonal variations. The mean CO_2 flux was 300.1 and $264.2 \text{ mmol m}^{-2} \text{ d}^{-1}$ during the wet season for large and small rivers, respectively, 2-fold larger than that during the dry season. ~~However, no significant difference in CO_2 flux was observed between small and large rivers.~~ The absence of commonly observed higher CO_2 fluxes in small rivers could be associated with the depletion effect caused by abundant and consistent precipitation in this subtropical monsoon catchment.

30 **1 Introduction**

River networks act as a processor that transfers and emits the carbon entering the water, rather than just a passive pipe that transports carbon from the terrestrial ecosystem to the ocean (Cole et al., 2007; Battin et al., 2009; Drake et al., 2018). CO₂ emissions at the water–air interface are an essential component of the riverine carbon cycle. CO₂ emitted from inland waters to the atmosphere reaches up to 2.9 PgC yr⁻¹,
35 surpassing that transported from land to ocean through rivers (Sawakuchi et al., 2017; Drake et al., 2018). Understanding the role that rivers play in the global carbon cycle is still hindered by uncertainty on the estimate of CO₂ flux outgassing from rivers (Cole et al., 2007; Raymond et al., 2013; Sawakuchi et al., 2017; Drake et al., 2018). Riverine carbon emissions have significant temporal and spatial variations, making it challenging to quantify carbon emissions accurately. In addition, watershed geomorphology,
40 hydrological conditions, climate, and other environmental factors can affect the CO₂ efflux in rivers (Alin et al., 2011; Abril et al., 2014; Almeida et al., 2017; Ran et al., 2017a; Borges et al., 2018). Thus, there are substantial differences in CO₂ efflux among rivers in different climate regions, or the same river but between different seasons (Denfeld et al., 2013; Rasera et al., 2013). An enhanced understanding of the temporal and spatial characteristics of the water–air CO₂ flux will facilitate a more robust estimate.
45 However, global riverine carbon emission estimates were largely based on data disproportionately focusing on temperate and boreal regions, including North America and Europe (Raymond et al., 2013; Lauerwald et al., 2015; Drake et al., 2018). In light of this data gap, more studies are required in other data-poor regions to achieve a more accurate estimate.

Rivers in tropical and subtropical regions of East Asia and Southeast Asia are among those
50 underrepresented regions that need more attention since they are essential participants in riverine carbon transport (Ran et al., 2015; Ran et al., 2017b; Drake et al., 2018). The high temperature in this region facilitated a high net primary productivity in the terrestrial ecosystem and intense biochemical activities, and both contributed to the carbon input dynamic from soil to rivers (Li et al., 2018). Meanwhile, rivers in this region are under the heavy influence of monsoon, and riverine CO₂ emissions vary significantly
55 among seasons due to the changes in temperature and precipitation. In addition, different rivers in this region may have contrasting trends in CO₂ dynamic due to different underlying controlling factors. Some rivers have the highest CO₂ efflux in the wet season (Li et al., 2013; Le et al., 2018; Ni et al., 2019), while others have the highest CO₂ efflux in the dry season (Luo et al., 2019) (~~Li et al., 2013; Le et al., 2018; Ni et al., 2019~~), suggesting that an increase in wet season runoff can have two distinct

60 consequences. One possibility is that it increases external carbon inputs and CO₂ emissions (Hope et al.,
2004; Johnson et al., 2008), while the other is that it leads to a dilution of CO₂ in rivers and accordingly
a reduction in CO₂ emissions (Ran et al., 2017b; Li et al., 2018). Since starkly different outcomes can
occur, it is important to investigate the processes behind such diverse response of rivers to the monsoon.

The Dongjiang River (DJR), located in the subtropical region of South China, is one of the three
65 tributaries of the Pearl River. Previous studies on riverine carbon transportation and emissions in the
Pearl rivers mainly focused on the Xijiang River, which was characterized by widely distributed
carbonate rocks, and the estuary area of the Pearl River Delta (Yao et al., 2007; Zhang et al., 2015; Zhang
et al., 2019; Liang et al., 2020). Though some studies have been conducted in the Dongjiang River basin
(DJRB) focusing on carbon transport and the carbon sink effect of chemical weathering (Tao et al., 2011;
70 Fu et al., 2014), there is still a lack of understanding of the characteristics of catchment-wide CO₂
emissions in DJRB. Furthermore, a predominantly hilly landscape combined with abundant precipitation
favors the formation of a great number of small rivers in DJRB (Ding et al., 2015). However, the current
estimate of basin-wide CO₂ emission from the river network was mostly based on the data from large
rivers, and small rivers are heavily underrepresented (Raymond et al., 2013; Drake et al., 2018). Because
75 the controlling factors and the input of carbon could be significantly different between large and small
rivers (Johnson et al., 2008; Dinsmore et al., 2013; Hotchkiss et al., 2015; Marx et al., 2017), which can
lead to very distinctive pattern of carbon dioxide evasion, ~~More~~ more comprehensive quantification of
CO₂ evasion from small headwater streams is necessary. Therefore, studies on the characteristics of
riverine CO₂ emission in DJRB should be conducted among river size spectrums, and the impact of
80 monsoon ought to be considered.

By using directly measured river water CO₂ partial pressure ($p\text{CO}_2$) and CO₂ efflux data from DJRB, and
in conjunction with hydrological and physicochemical data, the objectives of this study were to 1)
investigate the spatial and temporal pattern of $p\text{CO}_2$ and CO₂ emission along stream size spectrum, 2)
examine the differences in hydrological and physicochemical controls of $p\text{CO}_2$ and the CO₂ evasion
85 between small headwater streams and large rivers. The results of this study could shed light on the
underlying controls of the spatial and temporal distribution of riverine $p\text{CO}_2$ and support a refined
estimate of regional and global carbon budgets.

2 Material and methods

2.1 Site Description

90 The DJR in South China is one of the three major tributaries of the Pearl River system (Figure 1). It has a 562 km long mainstem channel and a drainage area of 35,340 km² (Chen et al., 2011). Due to its subtropical monsoon climate, precipitation in DJRB exhibits significant seasonal variability (Figure 2a). The multi-annual average precipitation is about 1800 mm, 80 % of which is concentrated during the wet season from April to September. The Boluo Hydrological Gauge is the lowermost gauge of the Dongjiang

95 River mainstem channel, controlling a drainage area of ~23,000 km². The multi-annual average water discharge at Boluo Hydrological Gauge is 23.7 km³ (Zhang et al., 2008). About 80–90 % of this discharge is transported during the wet season (Figure 2b). The landscape is characterized by plains and hills, accounting for 87.3 % of the river basin area (Ding et al., 2015), and ~~The~~ the dominant land use of the catchment is highly diverse evergreen forests of broad-leaved and needle-leaved species (Ran et al., 2012;

100 Chen et al., 2013). The impacts of human activities on land use vary among three regions in the DJRB. Urban expansion and agricultural activities have substantially altered the land use in Lower and Middle Dongjiang River Basin (LDJRB and MDJRB), respectively, while the Upper Dongjiang River Basin (UDJRB) is less affected by human activities (Figure 1), and the landscape is characterized by plains and hills, accounting for 87.3 % of the river basin area (Ding et al., 2015).

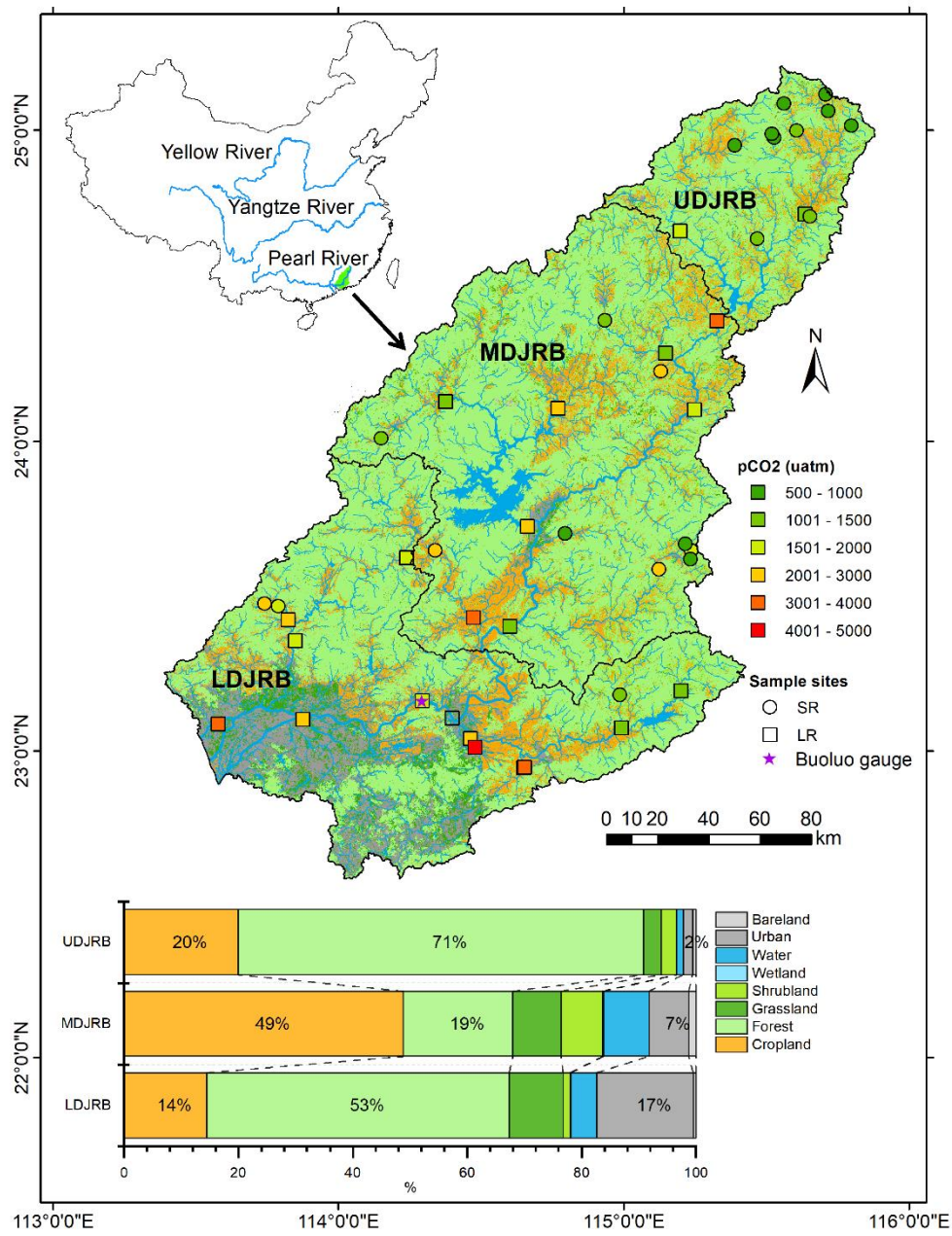


Figure 1 Location map of the Dongjiang River Basin, sampling sites, and Boluo Gauge.

Figure 1 Sample sites and land cover in the DJRB. Yearly average $p\text{CO}_2$ at each sample site was displayed. Based on land cover dataset: FROM-GLC10 (<http://data.ess.tsinghua.edu.cn>).

110

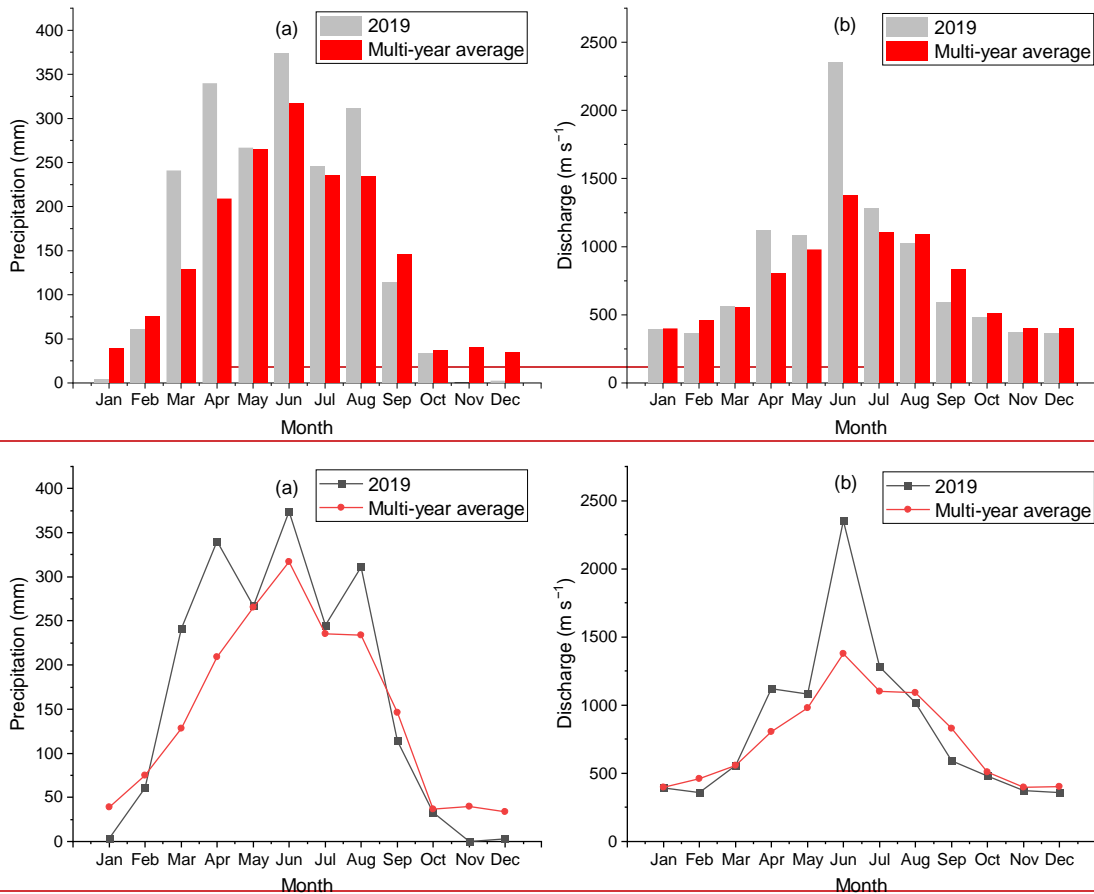


Figure 2 Monthly variations in (a) precipitation of the DJRB and (b) water discharge at the Boluo hydrological gauge, based on data provided by the Hydrological Bureau of Guangdong Province.

115

2.2 Field Measurement and Analysis

In total, there were 43 sampling sites ~~from spanning~~ seven Strahler stream orders. Fourth to seven order streams were mainstem and major tributaries, while first to third order streams were small tributaries. River widths were measured by a laser rangefinder. Sampled rivers were categorized, according to their stream orders, into small rivers (first to third order streams, SR) and large rivers (fourth to seventh order streams, LR). The small rivers had an average width of 15.4 ± 10.2 m (~~4.8 ± 2.3 m, 10.4 ± 5.6 m, 22.9 ± 8.1 m for first to third order streams, respectively~~), while large rivers have an average width of 180.8 ± 156.0 ~~180.3 ± 159.3 m (Table S1) (75.2 ± 51.0 m, 168.0 ± 48.6 m, 235.7 ± 29.6 m, 433.4 ± 178.0 m for fourth to seventh order streams, respectively)~~. Those sampling sites were widely distributed in the mainstem and nine major subcatchments among three regions with different topographic features and land cover (Figure 1).

In order to investigate CO₂ emissions during different hydrological conditions, we performed five fieldwork campaigns from December 2018 to October 2019, including three in the wet season (early wet season - late April, middle wet season - early July, and late wet season - late August) and two in the dry season (middle dry season - December 2018 to early January 2019 and early dry season - late October 2019). Sample sites were measured in the daytime over two weeks for each field trip. Three rounds of campaigns in the wet season allow each sample site to be measured under different hydrological conditions, and the two-week duration of each campaign allowed streams with different orders and sizes to be measured under various discharges. As for the dry season, the hydrological condition was relatively stable due to low precipitation. However, field measurements conducted during the daytime could lead to an underestimate in pCO₂ and CO₂ emission (Reiman and Xu, 2019a).~~In order to investigate CO₂ emissions during different hydrological conditions, we performed five fieldwork campaigns from December 2018 to October 2019, including late December 2018 to early January 2019 (middle dry season), April (early wet season), early July (middle wet season), late August (late wet season) and late October 2019 (early dry season). Nocturnal CO₂ emission rates in rivers could be 27% greater than the daytime rates (Gómez-Gener et al., 2021).~~

During the field trips, water temperature, pH, and dissolved oxygen (DO) were measured with a portable multiparameter probe (Multi 3430, WTW GmbH, Germany). The pH probe was calibrated before each field trip with standard pH buffers (4.01 and 7.00). Measurements were conducted 10 cm below the water

145 surface. To evaluate the contribution of metabolism on DO changes, ΔCO_2 and ΔO_2 were calculated as described by Stets et al. (2017) using:

$$\Delta\text{CO}_2 = \text{CO}_{2\text{w}} - \text{CO}_{2\text{a}} \quad (1)$$

and

$$\Delta\text{O}_2 = \text{O}_{2\text{w}} - \text{O}_{2\text{a}} \quad (2)$$

150 Where $\text{CO}_{2\text{w}}$ and $\text{O}_{2\text{w}}$ are measured concentrations of CO_2 and O_2 in water sample, while $\text{CO}_{2\text{a}}$ and $\text{O}_{2\text{a}}$ are the equilibrium CO_2 and O_2 concentrations ($\mu\text{mol L}^{-1}$).

Flow velocity was determined by using a Global Water Flow Probe FP111 with a precision of 0.1 m s⁻¹
~~Flow velocity was determined using a flow meter~~, while wind speed at 1.5 m above the water surface was measured with a Kestrel 2500 handheld anemometer and normalized to a height of 10 m (U10) using
155 the equation from Alin et al. (2011). As the flow velocity was measured near the riverbanks, an underestimation of the flow velocity is possible. Flow velocity measured near the riverbanks is only about 40% of the maximum flow velocity at the cross-section (Moramarco et al., 2004; Le Coz et al., 2008).

We also collected water for analyzing total alkalinity (TA) and dissolved organic carbon (DOC). Firstly,
160 100 ml of water samples were filtered through a pre-combusted glass fiber filter (pore size: 0.47 μm , Whatman GF/F, GE Healthcare Life Sciences, USA). Then, 50 ml of water used for TA analysis was titrated with 0.1 mol L⁻¹ HCl ~~at-on~~ the same day of sampling. The remaining 50 ml of water for DOC analysis was poisoned with concentrated H_2SO_4 to pH < 2 and preserved in a cooler with ice bags before analysis. DOC was determined by the high-temperature combustion method using a TOC Analyzer
165 (Elementar Analysensysteme GmbH, Langenselbold, Germany) that has a precision better than 3 %.

2.3 Calculation of $p\text{CO}_2$ and CO_2 emission flux

The surface water $p\text{CO}_2$ was determined using the headspace equilibrium method, which could avoid the possible overestimation of using TA and pH to calculate $p\text{CO}_2$ in rivers with a relatively low pH (Abril et al., 2015). We used a 625 mL reagent bottle to collect 400 mL of water from ~10 cm below the surface,
170 leaving 225 mL of space filled with ambient air as headspace. The bottle was then immediately capped and shaken vigorously for at least 1 min to achieve an equilibrium between the water and the CO_2 in the

headspace (Hope et al., 1994). Then, the bottle was connected to the calibrated Li-850 CO₂/H₂O gas analyzer (Li-Cor, Inc, USA), and the equilibrated gas in this closed loop was measured. The measurements at each site were repeated twice, and the average was then calculated. The variation between the two measurements was less than 5%, and the accuracy of Li-850 is within 1.5% of the reading. The ambient air pCO₂ (pCO₂^{air}) was measured before the headspace measurements and the chamber deployments. The pCO₂^{air} value varied between 380 and 450 μatm. The ambient air pCO₂ (pCO₂^{air}) was measured before the chamber deployments and varied between 380 and 450 μatm. The measurements at each site were repeated three times, and the average was then calculated. The original surface water pCO₂ (pCO₂^{water,i}) was finally calculated by using solubility constants (K₀) for CO₂ from Weiss (1974), Carbonate constants (K₁, K₂) from (Millero et al., 2006), and the volume of the flask, headspace, and residual system (line and gas analyzer) (Dickson et al., 2007; Ran et al., 2017a; Tian et al., 2019) using:

$$pCO_2^{water,i} = pCO_2^{headspace,f} + \left(\frac{V_h + V_r}{V_w}\right)(pCO_2^{h+r} - pCO_2^{headspace,i}) / [RTK_0 \left(1 + \frac{K_1}{[H^+]} + \frac{K_1 K_2}{[H^+]^2}\right)] \quad (3)$$

Where V_h , V_r and V_w , are the headspace volume, residence system volume, and water volume, respectively. R is the universal gas constant (8.314 J mol⁻¹ K⁻¹), T is the water temperature in Kelvin (K), and [H⁺] is the concentration of hydrogen ion. $pCO_2^{headspace,i}$ and $pCO_2^{headspace,f}$ are pCO₂ before and after the headspace equilibration, respectively. pCO_2^{h+r} is the pCO₂ of the mixed gas in the headspace and residual system during the measurement. the $pCO_2^{headspace,i}$ was taken as the pCO₂ in ambient air before the measurement, while $pCO_2^{headspace,f}$ was calculated using:

$$pCO_2^{headspace,f} = pCO_2^{h+r} + \left(\frac{V_r}{V_h}\right)(pCO_2^{h+r} - pCO_2^{headspace,i}) \quad (4)$$

For measuring V_r , We filled the headspace with gas, which had a known pCO₂, and measured the pCO₂ in the closed loop. V_r was then estimated according to equation (23). A comparative analysis of the syringe and bottle headspace method has been conducted to evaluate the accuracy of the headspace extraction method used in this study (Table S2 and Figure S2). Overall, our method could cause a 1–5% underestimation in pCO₂.

To reduce the artificial turbulence induced by anchored chambers, we used a small unmanned boat in the measurement, which allowed us to deploy drifting chambers freely in rivers deeper than 0.2 m and with

a high flow velocity up to 2 m s^{-1} . During the deployment, CO_2 emission was determined using a circular, 200 8.5 L floating chamber with a water surface area of 0.113 m^2 . The chamber walls were lowered about 2 cm into the water and mounted with a pneumatic rubber tire. The chamber was connected to an infrared Li-850 $\text{CO}_2/\text{H}_2\text{O}$ gas analyzer (Li-Cor, Inc, USA) in a floating storage box through Polyurethane tubes for CO_2 analysis. An unmanned boat connected to both the chamber and box with ropes was used to 205 deploy them near the central line of the river. Once the entire setup reached its designated location, the readings on the Li-850 were recorded at 0.5 s intervals. During the entire measurement process, the box drifted freely with the current. The Li-850 was calibrated by the manufacturer before field trips. The rate of CO_2 efflux (FCO_2 in $\text{mmol m}^{-2} \text{ d}^{-1}$) was calculated from the observed change rate of the mole fraction S (ppm s^{-1}) using:

$$\text{FCO}_2 = (S \cdot V / A) \cdot t_1 \cdot t_2 \quad (5)$$

210 Where S is the slope of CO_2 accumulation in the chamber ($\mu\text{atm s}^{-1}$), V is chamber gas volume (m^3), A is the chamber area (m^2), $t_1 = 8.64 \cdot 10^4 \text{ s d}^{-1}$ is the conversion factor from seconds to days, and t_2 is a conversion factor from mole fraction (ppm) to concentration (mmol m^{-3}) at in situ temperature (T in K) and atmospheric pressure (p in Pa), according to the ideal gas law:

$$t_2 = p / (8.31 \text{ J K}^{-1} \text{ mole}^{-1} \cdot T) \cdot 1000 \quad (6)$$

215 The gas transfer velocity (k) was calculated from FCO_2 and $p\text{CO}_2$ in both water and ambient air using:

$$k = \text{FCO}_2 / (K_0 \cdot (p\text{CO}_2^{\text{water},i} - p\text{CO}_2^{\text{air}})) \quad (7)$$

To compare gas transfer velocity values among different sites, k was standardized to k_{600} as described by Alin et al. (2011) using:

$$k_{600} = k (600 / Sc)^{-0.5} \quad (8)$$

220 Where, Sc is the Schmidt number, which is dependent on temperature (T) in degree Celsius (Wanninkhof, 1992):

$$Sc = 1911.1 - 118.11T + 3.4527T^2 - 0.4132T^3 \quad (9)$$

In total, 196 chamber measurements were made. In 19 out of 215 sample sites, the drifting chamber was unable to deploy due to shallow water or high flow velocity. Meanwhile, 8 out of 196 k_{600} data with the air–water $p\text{CO}_2$ gradient less than 200 μatm were also excluded, as the error in these calculations could be considerable (Borges et al., 2004).

3 Result

3.1 Physical and Biochemical Characteristics

The Dongjiang River was characterized by substantial seasonal variations in hydrologic regimes (Table Figure 2+). Stream width in the wet season was 17.0 % and 45.6 % larger than that in the dry season for small and large rivers, respectively (Table S1). The Q -discharge ranged 5–4 orders of magnitude from 0.01 $\text{m}^3 \text{s}^{-1}$ in the small headwater streams during the dry season to 6690 $\text{m}^3 \text{s}^{-1}$ in the main stem during the wet season (Figure S1). Water temperature was higher in July and August (21.4–33 and 21–33.4 °C, respectively) than that in January (8.1–22.2 °C), April (16.5–26.9 °C), and October (17.4–29.7 °C). pH varied from 6.38 to 8.14, with a mean of 7.08. There was no significant (independent sample t test, $p > 0.05$) change in pH between wet and dry seasons. U10 based on all stream sites was higher in large rivers (0.86 ± 0.91 and $1.43 \pm 1.58 \text{ m s}^{-1}$ in wet and dry season, respectively) than in small rivers (0.62 ± 0.61 and $0.76 \pm 0.73 \text{ m s}^{-1}$ in wet and dry season, respectively).

The streams presented low alkalinity ranging from 225 to 3025 $\mu\text{mol L}^{-1}$. Overall, lower alkalinity was observed in wet season than in dry season (Table 1). In small rivers, the alkalinity in wet season ($656 \pm 265 \mu\text{mol L}^{-1}$) was 21.1 % lower than the dry season ($831 \pm 460 \mu\text{mol L}^{-1}$), and the lowest alkalinity was observed in April ($615 \pm 262 \mu\text{mol L}^{-1}$), which was 30.4 % lower than in January ($883 \pm 548 \mu\text{mol L}^{-1}$). Similarly, the alkalinity in large rivers was $790 \pm 402 \mu\text{mol L}^{-1}$ in wet season, 14.5 % lower than $924 \pm 411 \mu\text{mol L}^{-1}$ in dry season. However, the lowest value of alkalinity in large rivers was observed in August ($739 \pm 312 \mu\text{mol L}^{-1}$) instead of April in small rivers.

Spatial and seasonal changes in DOC concentration were also observed in the surveyed rivers (Table 1). DOC concentration in large rivers ($1.94 \pm 1.52 \text{ mg L}^{-1}$) was 41.6 % higher than that in small rivers ($1.37 \pm 0.72 \text{ mg L}^{-1}$). Meanwhile, DOC concentrations in the wet season were $2.22 \pm 1.82 \text{ mg L}^{-1}$ and $1.54 \pm 0.72 \text{ mg L}^{-1}$ for large and small rivers, respectively, which were 45.1 % and 54 % higher than that in the dry season (1.53 ± 0.72 and $1.11 \pm 0.63 \text{ mg L}^{-1}$ for large and small rivers, respectively).

Table 1 Seasonal Variations of Physical and Biochemical Characteristics, expressed as Mean \pm SD.

Stream size	Season	Month	Water Temperature (°C)	pH	Alkalinity ($\mu\text{mol L}^{-1}$)	DOC (mg L^{-1})
<i>small</i>	Dry	January	14.3 \pm 4.1	7.05 \pm 0.31	883 \pm 548	1.07 \pm 0.37
	Wet	April	19.9 \pm 1.9	7.19 \pm 0.26	615 \pm 262	1.51 \pm 0.58
	Wet	July	25.7 \pm 2.3	7.17 \pm 0.27	676 \pm 227	1.59 \pm 0.97
	Wet	August	27.1 \pm 3.0	7.13 \pm 0.38	678 \pm 308	1.51 \pm 0.56
	Dry	October	21.5 \pm 2.6	7.08 \pm 0.23	778 \pm 358	1.16 \pm 0.82
<i>large</i>	Dry	January	16.9 \pm 5.5	7.00 \pm 0.27	961 \pm 409	1.70 \pm 1.52
	Wet	April	22.1 \pm 3.7	7.20 \pm 0.27	890 \pm 386	2.22 \pm 1.65
	Wet	July	27.8 \pm 2.9	6.92 \pm 0.25	740 \pm 305	1.97 \pm 1.77
	Wet	August	28.9 \pm 3.3	6.92 \pm 0.26	739 \pm 312	2.47 \pm 2.04
	Dry	October	25.2 \pm 3.1	7.13 \pm 0.29	887 \pm 331	1.37 \pm 0.67

3.2 Spatial and Seasonal variation in $p\text{CO}_2$

255 3.2 Spatial and Seasonal variation in $p\text{CO}_2$

The $p\text{CO}_2$ ranged from 15 to 6323 μatm with a catchment-wide average of 1748 μatm and showed considerable temporal and spatial variation throughout the sampling period. There was an increasing trend of observed $p\text{CO}_2$ from *small* to large rivers (Figure 3a). On average, the $p\text{CO}_2$ values were 856 \pm 444, 1481 \pm 979, 1354 \pm 753, 2332 \pm 1330, 2142 \pm 1016, 2271 \pm 1121, and 2168 \pm 1046 μatm for streams from first to seventh order, respectively (Figure 3a). The stronger increase in $p\text{CO}_2$ occurred between third and fourth order streams (from 1354 \pm 753 to 2332 \pm 1330 μatm , Figure 3a). Overall, $p\text{CO}_2$ in large rivers (2250 \pm 1178 μatm) was 76.3 % higher than that in small rivers (1276 \pm 796 μatm). Meanwhile, there was also an increasing trend of $p\text{CO}_2$ from rivers in UDJRB to those in LDJRB. The $p\text{CO}_2$ values were 2105 \pm 959 and 2487 \pm 1276 μatm for small and large rivers respectively in LDJRB, which were 146.7% and 70% higher than that in UDJRB, respectively (Figure 3b).

260

265

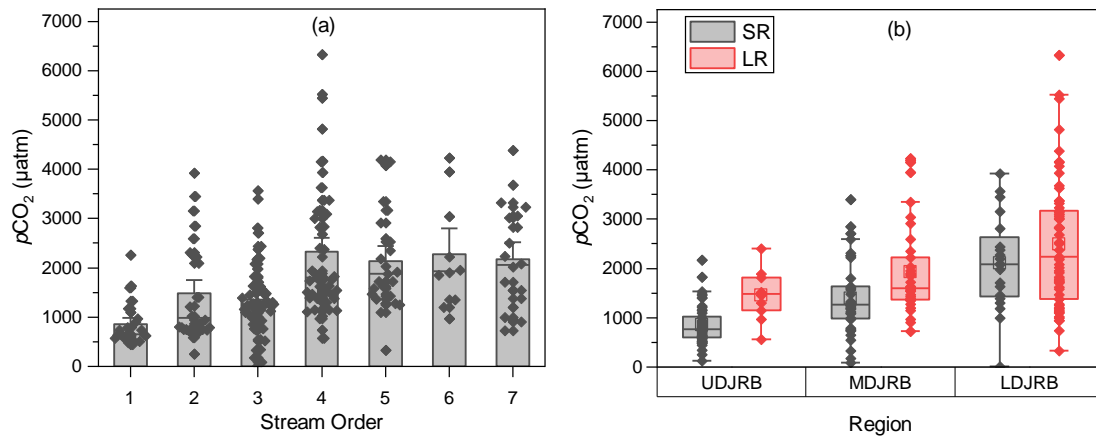
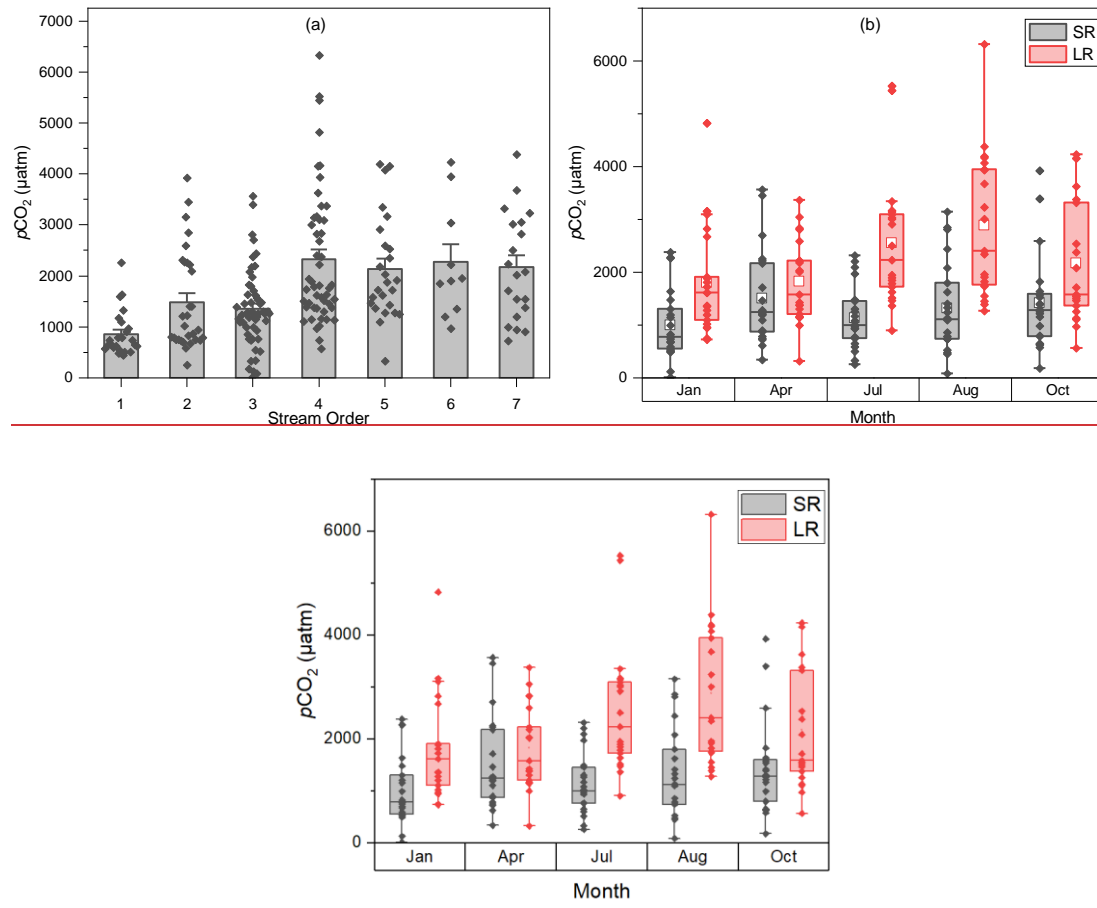


Figure 3 Spatial variations in $p\text{CO}_2$. (a) Yearly average $p\text{CO}_2$ in the seven stream orders, standard errors (SE) are displayed by error bars. (b) Measured $p\text{CO}_2$ in small and large rivers among three regions in the DJRB. The box mid-lines represent medians; the interquartile range (IQR) is represented by top and bottom of the box, respectively; whiskers indicate the range of 1.5 IQR; the white square symbols represent means, and the other symbols represent $p\text{CO}_2$ values for each sampled site.

Seasonal variations of $p\text{CO}_2$ differ across the stream size spectrum (Figure 3b4). In small rivers, the highest $p\text{CO}_2$ was observed in April ($1506 \pm 880 \mu\text{atm}$), which was 50.3 % higher compared to-w~~ith~~ January ($1002 \pm 660 \mu\text{atm}$). $p\text{CO}_2$ then decreased in July ($1131 \pm 589 \mu\text{atm}$) and increased in August ($1325 \pm 863 \mu\text{atm}$) and October ($1414 \pm 900 \mu\text{atm}$). Compared to-w~~ith~~ small rivers, the peak of $p\text{CO}_2$ in large rivers occurred later but persisted for a longer period of time. In large rivers, an increase in $p\text{CO}_2$ was not observed until July. $p\text{CO}_2$ in April was $1831 \pm 793 \mu\text{atm}$, which was similar to $1805 \pm 1010 \mu\text{atm}$ in January, and it increased 39.3 % to $2550 \pm 1210 \mu\text{atm}$ in July. $p\text{CO}_2$ peaked in August ($2885 \pm 1351 \mu\text{atm}$) and then decreased to 2176 ± 1166 in October. Overall, $p\text{CO}_2$ was 9.3 % and 21.7 % higher in wet season than in dry season for small and large rivers, respectively.



285 **Figure 3** Spatial and Seasonal variations in $p\text{CO}_2$. (a) Yearly average $p\text{CO}_2$ in the seven stream orders, standard errors (SE) are displayed by error bars. (b) Seasonal $p\text{CO}_2$ in small and large rivers. The box mid-lines represent medians; the interquartile range (IQR) is represented by top and bottom of the box, respectively; whiskers indicate the range of 1.5 IQR; the white square symbols represent means, and the other symbols represent $p\text{CO}_2$ values for each sampled site.

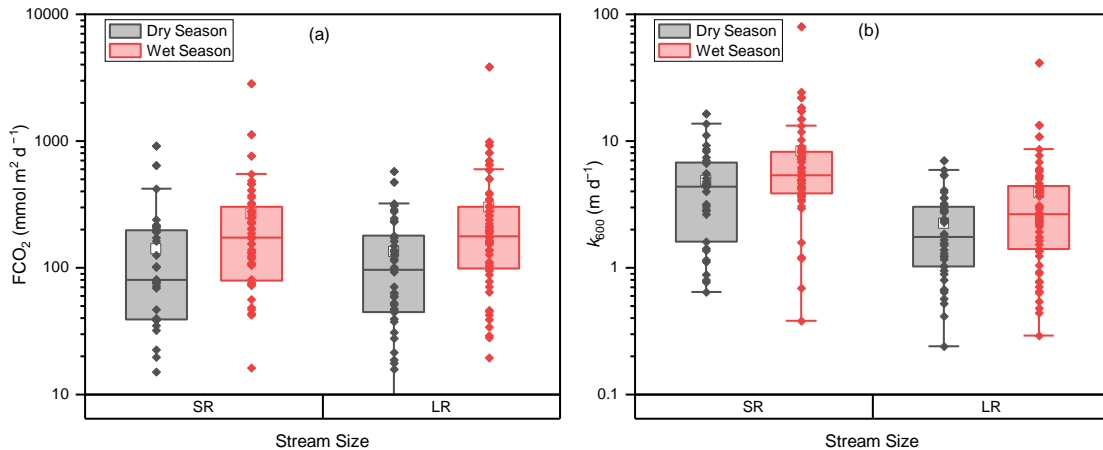
290 3.3 CO_2 effluxes and k_{600}

CO_2 effluxes ranged from -129.8 to $3874.8 \text{ mmol m}^{-2} \text{ d}^{-1}$ with a mean of $225.2 \text{ mmol m}^{-2} \text{ d}^{-1}$. More than 95 % of the 196 samples had positive FCO_2 values, indicating that the majority of the surveyed rivers is a carbon source. Overall, we observed higher FCO_2 during wet season than during dry season in both small and large rivers (Figure 4a5a). FCO_2 in small rivers and large rivers were 264.2 ± 410.0 and 300.1

295 $\pm 511.7 \text{ mmol m}^{-2} \text{ d}^{-1}$ respectively during the wet season, which was 87.2 % and 123.1 % higher compared to than that in the dry season (141.1 ± 188.7 and $134.5 \pm 129.5 \text{ mmol m}^{-2} \text{ d}^{-1}$ for small and large rivers respectively). No significant (independent sample t test, $p > 0.05$) difference in FCO_2 was observed between small and large rivers.

300 k_{600} differs greatly between river size classes and among hydrological periods (Figure 5b4b). k_{600} values in small rivers were significantly (independent sample t test, $p < 0.001$) higher on average than in large rivers. The mean values of k_{600} in small rivers were $8.29 \pm 11.29 \text{ m d}^{-1}$ and $4.90 \pm 3.82 \text{ m d}^{-1}$ for the wet season and dry season, respectively, which were 112.6 % and 70 % higher than that of large rivers ($3.90 \pm 5.55 \text{ m d}^{-1}$ in the wet season and $2.25 \pm 1.61 \text{ m d}^{-1}$ in the dry season). k_{600} during the wet season were also significantly (independent sample t test, $p < 0.05$) higher than the dry season. k_{600} increased 112.7 % and 118.2 % from dry season to wet season in small and large rivers, respectively. However, comparisons between different phases in the same hydrological period (e.g. early, middle, and late wet season) did not differ significantly (paired sample t test, $p > 0.05$) for both river size classes.

The spatial and temporal variation of CO_2 efflux generally coincided with the changes in $p\text{CO}_2$ and k_{600} since high FCO_2 occurred when k_{600} or $p\text{CO}_2$ were elevated. In small rivers, the highest CO_2 effluxes were $346.8 \pm 625.2 \text{ mmol m}^{-2} \text{ d}^{-1}$ during April, consistent with the high k_{600} and $p\text{CO}_2$ in this period. In large rivers, high CO_2 effluxes were observed in both April ($339.9 \pm 828.6 \text{ mmol m}^{-2} \text{ d}^{-1}$) and August ($329.9 \pm 270.0 \text{ mmol m}^{-2} \text{ d}^{-1}$), which were attributed to high k_{600} in April and high $p\text{CO}_2$ in August.



315 **Figure 4.5** Relationship between stream size and (a) FCO_2 and (b) k_{600} . -The box mid-lines represent medians; the interquartile range (IQR) is represented by top and bottom of the box, respectively; whiskers indicate the range of 1.5 IQR; the white square symbols represent means, and the other symbols represent FCO_2 and k_{600} values for each sampled site.

4 Discussions

4.1 Underlying Processes of pCO_2 dynamics

320 ~~Previous studies show that riverine CO_2 originated from both lateral soil CO_2 input and in stream metabolism (Yao et al., 2007; Li et al., 2013; Abril et al., 2014). The river water pCO_2 was positively related to DOC and negatively related to DO (Figure 5), indicating that decomposition of terrestrial organic carbon is an important source for pCO_2 (Stets et al., 2017; Liang et al., 2020). To compare the contribution of internal metabolism on pCO_2 in small and large rivers, $\Delta CO_2 : \Delta O_2$ stoichiometry was used to evaluate the impact of respiration and photosynthesis processes on the concentration of O_2 and CO_2 in water bodies (Stets et al., 2017). The inverse relation between ΔCO_2 and ΔO_2 (Figure 6) demonstrated that metabolic processes are important for CO_2 variation (Amaral et al., 2020). However, the imbalanced $\Delta CO_2 : \Delta O_2$ stoichiometry (Figure 6) indicates that, in addition to in stream metabolic processes, other factors also affect the CO_2 and O_2 in the water (Stets et al., 2017). For example, 183 out of 215 observations are above the 1:1 $\Delta CO_2 : \Delta O_2$ line, suggesting additional sources of carbon input. The difference in the $\Delta CO_2 : \Delta O_2$ stoichiometry between small and large rivers reflects their differences in the controlling processes (Rasera et al., 2013). In large rivers, the $\Delta CO_2 : \Delta O_2$ stoichiometry is closer to the 1:1 line than in small rivers, suggesting large rivers are more affected by the metabolic processes (Jeffrey et al., 2018; Amaral et al., 2020). In comparison, the deviation from the 1:1 line in small rivers indicates a stronger impact of additional carbon sources (Abril et al., 2014; Amaral et al., 2020).~~

The spatial pattern of pCO_2 in the DJRB is likely resulting from changes in the intensity of in-stream metabolism. Our data showed that river water pCO_2 was negatively related to DO and positively related to DOC (Figure 6), suggesting that metabolic processes are important for CO_2 variation (Amaral et al., 2020). High pCO_2 and low DO in large rivers could result from more favorable conditions for OC composition. Terrestrial organic carbons are difficult to convert into CO_2 in small rivers due to the high flow velocity and short water residence time (Hotchkiss et al., 2015). Conversely, a greater fraction of OC could be transported and fuel the heterotrophic respiration in large rivers, where low flow velocity

340

and long water residence time facilitated the decomposition of organic carbon within the water column (Denfeld et al., 2013).

345

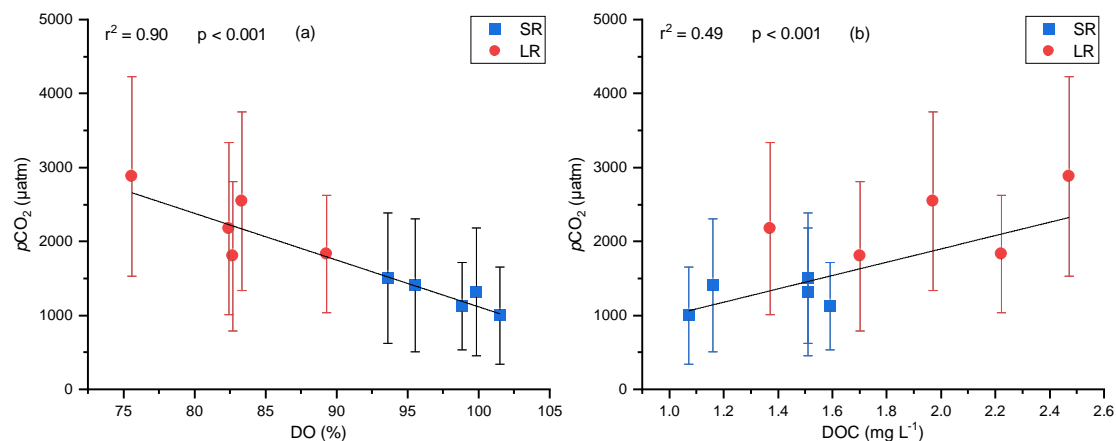
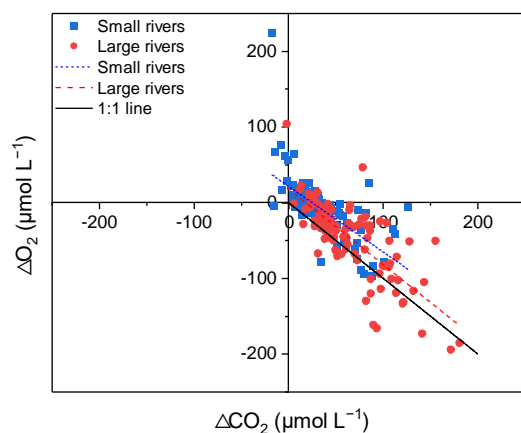


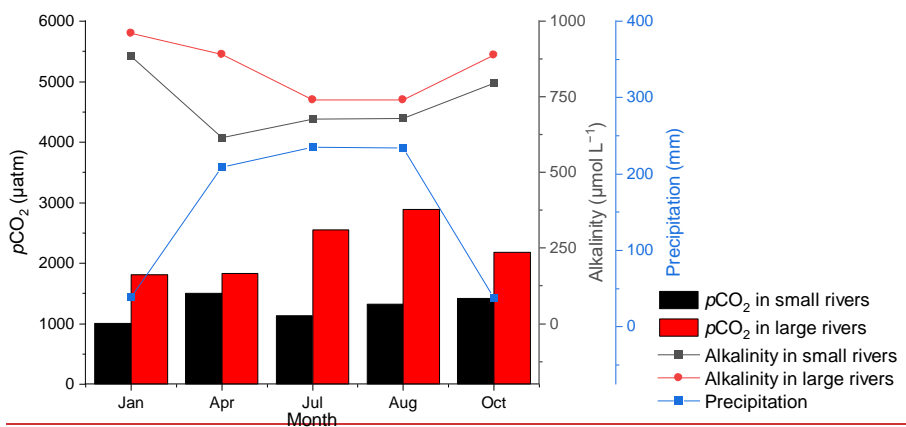
Figure 5-6 Relationship between seasonal average $p\text{CO}_2$ and (a) DO and (b) DOC. Error bars for the $p\text{CO}_2$ represent 1 standard deviation from the seasonal mean. The DO- $p\text{CO}_2$ and DOC- $p\text{CO}_2$ relationship are shown as solid lines.



350 **Figure 6** The relationship between ΔCO_2 and ΔO_2 . Points greater than zero are oversaturated, and less than zero are undersaturated. Points above the 1:1 line would have extra carbon sources in addition to in-stream metabolic processes.

355 Differences in seasonal changes of $p\text{CO}_2$ between small and large rivers also suggest various primary controlling processes. $p\text{CO}_2$ in small rivers are mainly controlled by changes in lateral soil CO_2 input. The highest value of $p\text{CO}_2$ observed in April could be attributed to a rapid surge of additional soil CO_2 input caused by increasing precipitation (Figure 7). In spring, warming temperatures increase the net primary productivity of the terrestrial ecosystem, with a corresponding increase in soil carbon content. Meanwhile, increased precipitation in April

360 facilitates the transportation of the soil carbon from land to the river system (Rasera et al., 2013). Thus, the temperature and precipitation in April dominantly control the soil CO₂ concentration, and hence mediate aqueous pCO₂ (Hope et al., 2004; Yao et al., 2007; Johnson et al., 2008). In contrast, a decrease of pCO₂ in July was observed, and it was likely the result of the CO₂ depletion effect in the soil combined with the dilution effect of precipitation. The soil carbon has experienced a depletion effect due to the continuous precipitation and soil erosion since April, limiting the supply of terrestrial carbon input for rivers in July (Hope et al., 2004; Johnson et al., 2007; Dinsmore et al., 2013). Meanwhile, the increase in precipitation and runoff can also cause a dilution effect, which leads to a decrease of pCO₂ (Ran et al., 2017b; Li et al., 2018). (Hope et al., 2004) Seasonal variations in alkalinity substantiate the dilution effect and the depletion effect in July. Although the lowest alkalinity in small rivers was recorded in April, the highest pCO₂ values in small rivers were recorded in that month. It suggests that the effect of increased soil CO₂ input outweighs the dilution effects, both of which are caused by precipitation increase. In contrast, the synchronous upward trend of the alkalinity and pCO₂ in the later months of the year implies that the rise in pCO₂ results from weakened dilution effect (Ni et al., 2019). Moreover, low pCO₂ during dry season demonstrates inorganic carbon input via groundwater plays a minor role. Therefore, the variation of soil CO₂ input and dilution effect caused by precipitation are the main controlling factors of seasonal changes in riverine CO₂ among small rivers.

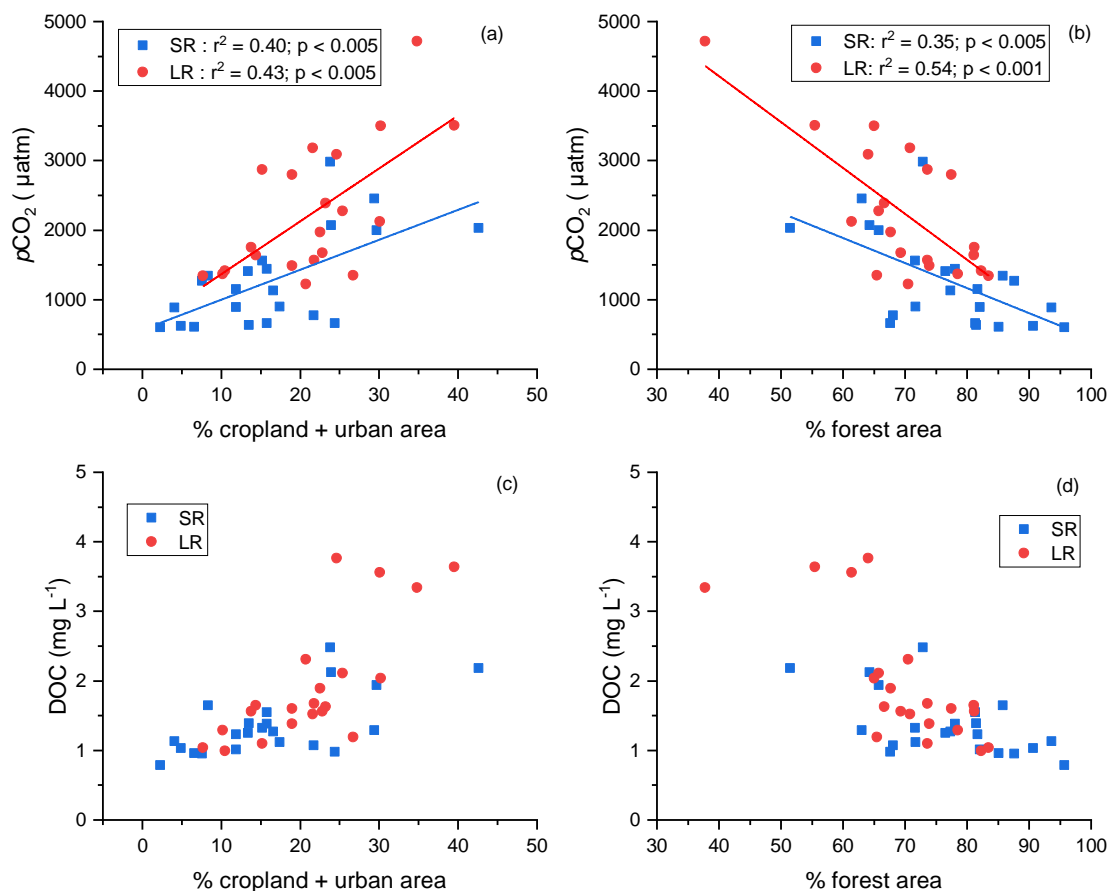


375 **Figure 7 Seasonal variations of pCO₂, alkalinity, and precipitation.**

380 The spatial pattern of pCO₂ was also related to the variation in carbon input due to different land cover (Borges et al., 2018). The higher pCO₂ in large rivers than small rivers was associated with a higher percentage of urban and cropland cover and lower forest cover (Figure S3). Compared with the forest, cropland could provide a more favorable condition for soil erosion and the transfer of organic matter from land to rivers, contributing to a higher pCO₂. Intensification of agricultural practices could promote the decomposition of soil organic matter (Borges et al., 2018) and increase the concentration of liable DOC, which is more sensitive to in-stream metabolism after entering the rivers (Lambert et al., 2017; Li et al., 2019). Meanwhile, the input of wastewater with high organic matter concentration from the urban area could also contribute to an increase in riverine pCO₂ (Xuan et al., 2020; Zhang et al., 2021).

385 Moreover, our result showed increasing $p\text{CO}_2$ from forest-dominated streams in UDJRB to those in
agricultural and urban impacted catchments in MDJRB and LDJRB (Figure 3b). Over 70% of forest
cover in UDJRB (Figure 1) can reduce the soil erosion associated with precipitation (Ran et al., 2018).
Meanwhile, the organic matter from forest tend to be more aromatic, thus more capable of surviving
390 biodegradation (Kalbitz and Kaiser, 2008), leading to a relatively low riverine $p\text{CO}_2$ value. In contrast,
cropland, occupying about 49% of the land cover (Figure 1), was the primary land use type in the MDJRB
substituting forest, and urban areas accounting for about 17% of the land cover in the LDJRB. The higher
 $p\text{CO}_2$ in the MDJRB and LDJRB is likely under the influence of agricultural practices and wastewater
input. Overall, land use mainly affects the spatial distribution of $p\text{CO}_2$ by altering the amount and lability
of carbon inputs to the rivers.

395 However, DOC concentration is not likely the primary control of different in-stream metabolism
intensities in small and large rivers. Our result showed that large rivers had similar DOC concentration
but higher $p\text{CO}_2$ compared with small rivers with similar land cover (Figure 7) when the percentage of
forest area was over 65% or the percentage of combined cropland and urban area was less than 30%.
This suggested that large rivers have more intense OC decomposition than small rivers with similar DOC
400 concentrations. Therefore, favorable conditions for OC decomposition were more likely to be responsible
for the spatial pattern. Another possible carbon source of river water CO_2 is direct soil CO_2 input.
However, it is unlikely the major contributor of CO_2 for large rivers in the DJRB, since the contribution
of soil CO_2 tends to decrease with the increased stream order and leads to higher $p\text{CO}_2$ in small rivers
(Marx et al., 2017), which contradicted with the spatial pattern in this study.



405 **Figure 7** (a) the relationship between yearly average $p\text{CO}_2$ at each site and the percentage of cropland and urban
 410 area combined (b) the relationship between yearly average $p\text{CO}_2$ at each site and the percentage of forest area (c)
 the relationship between yearly average DOC at each site and the percentage of cropland and urban area combined
 (d) the relationship between yearly average DOC at each site and the percentage of forest area. On the other hand,
 high $p\text{CO}_2$ in large rivers is mainly a consequence of decomposition of organic carbon. Relatively low $p\text{CO}_2$ in April
 indicates a carbon source other than soil CO_2 input. When soil carbon dioxide enters river systems, it is readily
 emitted from the rivers into the air, with little reaching the larger rivers downstream (Denfeld et al., 2013; Drake et
 al., 2018). The contribution of soil CO_2 input to $p\text{CO}_2$ could only be secondary. In large rivers, $p\text{CO}_2$ increased by
 39.3 % from $1831 \pm 793 \mu\text{atm}$ in April to $2550 \pm 1210 \mu\text{atm}$ in July. The rise in temperature from April to July
 promoted a substantial increase in the net primary productivity of the terrestrial ecosystem and the content of
 415 terrestrial organic carbon entering the river (Borges et al., 2018). (Vonk et al., 2013; Dean et al., 2019) Yet, those
 terrestrial organic carbons are difficult to convert into CO_2 in small rivers due to the high flow velocity and short
 water residence time (Hotchkiss et al., 2015). Thus, a possible explanation of increasing $p\text{CO}_2$ in large river is that a
 greater fraction of OC could be transported and fuel the heterotrophic respiration in large rivers, where long water
 residence time combined with the high temperature in July facilitate OC decomposition (Denfeld et al., 2013). For
 420 large rivers, recent studies have shown that the biological decomposition of allochthonous organic carbon caused by
 energetic microbial metabolism is the primary source of riverine CO_2 (Amaral et al., 2018; Jeffrey et al.,
 2018). (Borges et al., 2018) (Ran et al., 2018) (Borges et al., 2018) (Lambert et al., 2017; Li et al., 2019) (Xuan et al.,
 2020; Zhang et al., 2021)

425 On the other hand, the temporal pattern is likely the consequence of changes in terrestrial carbon input
and in-stream metabolism intensity. Our result showed that higher $p\text{CO}_2$ occurred in the wet season than
the dry season for both small and large rivers (Figure 4). The elevated temperature in the wet season
could promote a substantial increase in the net primary productivity of the terrestrial ecosystem, while
increased precipitation facilitated the transfer of terrestrial carbon (Rasera et al., 2013), including both
soil CO_2 and OC, from land to rivers. This could either enhance riverine $p\text{CO}_2$ directly or by fuelling OC
430 decomposition (Borges et al., 2018). However, differences in seasonal changes of $p\text{CO}_2$ between small
and large rivers (Figure 4) also suggested that their primary controlling process could be different. For
small rivers, the highest value of $p\text{CO}_2$ was observed in April (Figure 4), which is consistent with the
rapid surge of terrestrial C input, usually occurring at the beginning of the wet season (Hope et al., 2004;
Yao et al., 2007; Johnson et al., 2008). However, such an increase in $p\text{CO}_2$ was not observed in large
435 rivers (Figure 4), even though DOC in large rivers, increased during the same period, similar to small
rivers (Table 1). A possible explanation is that observed $p\text{CO}_2$ rise was mainly originated from soil CO_2 ,
which was readily emitted from the small rivers into the air, with little reaching the larger rivers
downstream (Denfeld et al., 2013; Drake et al., 2018). Differences in $p\text{CO}_2$ dynamic in July and August
also reflected differential controlling processes in small and large rivers. A decline in $p\text{CO}_2$ in July in
440 small rivers suggested that it might have experienced the depletion effect occurring at middle and late
wet season (Hope et al., 2004), during which soil CO_2 decreased due to the continual precipitation. In
contrast, the increase in $p\text{CO}_2$ occurring in large rivers in July indicated that the decrease in soil CO_2
input could hardly affect the $p\text{CO}_2$ in large rivers during this period. Instead, stronger in-stream
metabolism caused by OC input and favorable conditions for OC decomposition is more likely to be
445 responsible for the rising $p\text{CO}_2$.

To compare the contribution of internal metabolism on $p\text{CO}_2$ in small and large rivers, ΔCO_2 : ΔO_2
stoichiometry was used to evaluate the impact of respiration and photosynthesis processes on the
concentration of O_2 and CO_2 in water bodies (Stets et al., 2017). The inverse relation between ΔCO_2 and
 ΔO_2 (Figure 8) demonstrated that metabolic processes are important for CO_2 variation (Amaral et al.,
450 2020). It is also supported by the positive relation between river water $p\text{CO}_2$ and DOC and the negative
relation between $p\text{CO}_2$ and DO (Figure 6). However, the imbalanced ΔCO_2 : ΔO_2 stoichiometry (Figure
7) indicates that, in addition to in-stream metabolic processes, other factors also affect the CO_2 and O_2 in
the water (Stets et al., 2017). For example, 183 out of 215 observations were above the 1:1 ΔCO_2 : ΔO_2

455 line, suggesting additional sources of carbon input. The difference in the $\Delta\text{CO}_2:\Delta\text{O}_2$ stoichiometry
between small and large rivers reflects their differences in the controlling processes (Rasera et al., 2013).
In large rivers, the $\Delta\text{CO}_2:\Delta\text{O}_2$ stoichiometry is closer to the 1:1 line than in small rivers, suggesting large
rivers are more affected by the metabolic processes (Jeffrey et al., 2018; Amaral et al., 2020). In
comparison, the deviation from the 1:1 line in small rivers indicates a stronger impact of external carbon
sources (Abril et al., 2014; Amaral et al., 2020), which substantiates our finding that $p\text{CO}_2$ of small rivers
460 are more likely affected by soil CO_2 input. Furthermore, there were other processes that could affect the
riverine $p\text{CO}_2$. For example, stronger solar radiation during summer could increase photo-oxidation in
rivers. However, commonly observed lower daytime CO_2 emission rates than nocturnal rates (Gómez-
Gener et al., 2021) suggests that photosynthesis overrides photo-oxidation in CO_2 dynamics. Nonetheless,
the low DO concentration observed in the surveyed rivers (Figure 8) suggested that photosynthesis is not
465 the primary control of the seasonal variation of $p\text{CO}_2$.

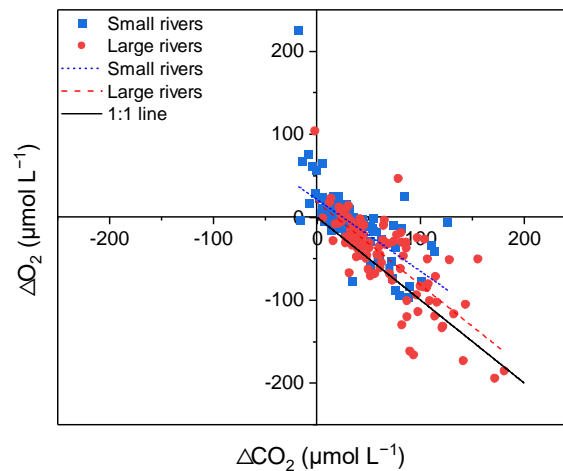


Figure 8 The relationship between ΔCO_2 and ΔO_2 . Points greater than zero are oversaturated, and less than zero are undersaturated. Points above the 1:1 line indicate the existence of additional carbon sources, apart from in-stream metabolic processes.

470 **4.2 Environmental Control of k_{600} variation**

Environmental factors, including wind speed and hydrological variables, could affect the gas exchange at the water–air interface and were typically used to explain the variance in k_{600} (Alin et al., 2011; Raymond et al., 2012). Flow velocity generally determine the k_{600} in rivers, while wind speed becomes a

more important factor in controlling the k_{600} in large rivers, reservoirs and estuary (Guérin et al., 2007; 475 Rasera et al., 2013; Amaral et al., 2020). In our surveyed rivers, k_{600} displayed a significant linear correlation (Pearson correlation, $p < 0.001$) with the flow velocity. Our k_{600} model (Figure 8) base on 188 field measurement data is similar to that developed by Alin et al. (2011) ($k_{600} = 13.82 + 0.35v$). However, in our studied rivers, no significant correlation (Pearson correlation, $p > 0.05$) was found between wind speed and k_{600} regardless of stream size. This could be explained by the lower wind speed 480 (Table 2, $0.68 \pm 0.66 \text{ m s}^{-1}$ and $1.09 \pm 1.06 \text{ m s}^{-1}$ for small and large rivers, respectively) (Guérin et al., 2007). As the wind speed decreases, the impact of flow velocity on k_{600} will increase considerably (Borges et al., 2004). Therefore, the accuracy of k_{600} estimation based on wind speed in nearby regions should be examined using measurement data (Yao et al., 2007; Li et al., 2018). The temporal heterogeneities of k_{600} between small and large rivers reveal the differences in flow regime. k_{600} in small 485 rivers are significantly (independent sample t test, $p < 0.001$) higher than in large rivers, which could be explained by higher flow velocity in small rivers due to a higher gradient. Meanwhile, significantly higher k_{600} (independent sample t test, $p < 0.05$) was also observed in the wet season compared ~~to~~with the dry season, which is the result of increasing flow velocity and turbulence due to plentiful monsoon-induced precipitation during wet season (Guérin et al., 2007; Alin et al., 2011; Ho et al., 2018).

490

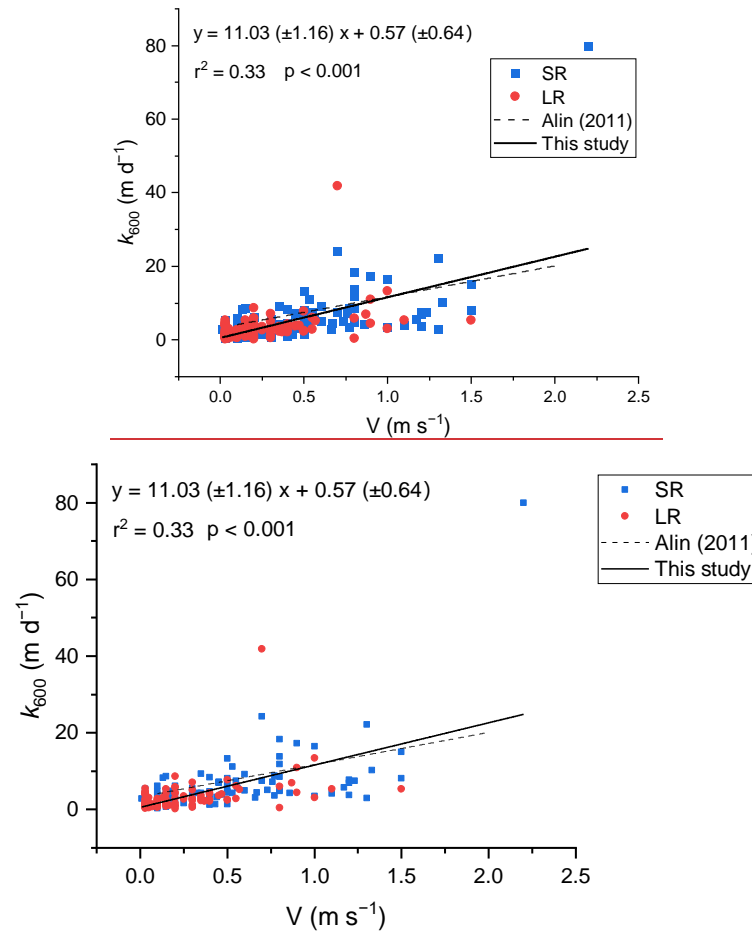


Figure 8-9 Relationship between k_{600} and flow velocity. The dashed line represents the parameterization of Alin et al (2011).

Table 2. Seasonal variation of k_{600} and environmental factors in small and large rivers.

Stream size	Season	Current velocity (m s ⁻¹)	U10 (m s ⁻¹)	k_{600} (m d ⁻¹)
small	Wet	0.66 ± 0.47	0.62 ± 0.61	8.29 ± 11.29
	Dry	0.43 ± 0.27	0.76 ± 0.73	4.90 ± 3.82
large	Wet	0.32 ± 0.32	0.86 ± 0.91	3.90 ± 5.55
	Dry	0.17 ± 0.19	1.43 ± 1.58	2.25 ± 1.61

495

Exceptionally high k_{600} values were observed in the surveyed rivers (Figure 89). The highest k_{600} in large and small rivers were 41.83 and 79.97 m d^{-1} , which were 5-fold and 3-fold larger than calculated k_{600} , respectively. This is the result of the exponential increase in k_{600} due to extreme flood events. Generally, flood events associated with heavy rainfall during the wet season can increase flow velocity and turbulence at the water–air interface (Almeida et al., 2017; Geeraert et al., 2017), leading to substantially higher k_{600} . Yet, neither our model nor the one from Alin et al. (2011) was suitable for the estimation of k_{600} during extreme flood events because the calculated k_{600} could deviate far from the measured k_{600} when they occurred. Therefore, the extent to which flood events affect k_{600} and riverine CO_2 emission is still uncertain and warrant continued research (Drake et al., 2018).

505 4.3 A Comparison of CO_2 Emissions to Other Rivers

The mean CO_2 fluxes of 225.2 $\text{mmol m}^{-2} \text{d}^{-1}$ in DJRB is comparable to those observed in tropical and subtropical rivers in the Americas, Africa, and Southeast Asia (Table 3). Although the magnitude of the CO_2 evasion of these river basins is similar, the seasonal variations and drivers behind them could differ. The higher CO_2 emission in the Dongjiang Basin was observed in the wet season compared to the dry season, and this seasonal pattern is similar to that observed in the Xijiang and Daning rivers (Yao et al., 2007; Ni et al., 2019) but different from the one from Jinshui River in the upper reaches of the Yangtze River, where $p\text{CO}_2$ is high in winter and low in summer (Luo et al., 2019), even though all four rivers are in the East Asia Monsoon climate region. The difference in seasonal pattern can be explained by the drivers of $p\text{CO}_2$ variability as the seasonal variation of riverine $p\text{CO}_2$ is ~~the likely resulting from result of~~ the ~~increase changes~~ of ~~external CO_2 input~~ carbon input, internal production of CO_2 (Yao et al., 2007), and the dilution effect caused by precipitation (Johnson et al., 2007). For rivers where $p\text{CO}_2$ is lower in summer than in winter, the dilution effect overrides the effect of increased carbon inputs ~~and internal CO_2 production~~ (Luo et al., 2019). In contrast, for rivers like the Dongjiang river, although the dilution effect remains, increased CO_2 input and metabolism are more significant factors in controlling $p\text{CO}_2$, thus leading to higher summer $p\text{CO}_2$. In addition, the controlling processes of the Dongjiang River may be different even when compared ~~to~~ ~~with~~ rivers with similar seasonal variations in the same climatic zone. For instance, DO in the Xijiang river was supersaturated, indicating that photosynthetic activities in the water body mainly reduce the CO_2 concentration in the rivers (Yao et al., 2007). Therefore, other carbon sources like soil respiration and carbonate weathering should be responsible for high $p\text{CO}_2$ in summer (Zhang et al., 2019). In contrast, low DO value and a negative correlation between DO and $p\text{CO}_2$

have been observed in the Dongjiang River, indicating that photosynthesis is relatively weak compared with the respiration in the water body-, and the latter one is an essential source of riverine CO₂ (Stets et al., 2017) ~~and results-resulting~~ in higher pCO₂ in summer.

Table 3. Comparison of CO₂ emission in subtropical and tropical rivers.

<u>Rivers</u>	<u>Climate</u>	<u>Season</u>	<u>pCO₂</u> <u>(μatm)</u>	<u>k₆₀₀</u> <u>(m d⁻¹)</u>	<u>FCO₂</u> <u>(mmol m⁻² d⁻¹)</u>	<u>References</u>
The Dongjiang River (Large rivers)	Subtropical	Wet	2422 ± 1209	3.90 ± 5.55	300.1 ± 511.8	This study
		Dry	1990 ± 1094	2.25 ± 1.61	134.5 ± 129.5	
The Dongjiang River (small rivers)	Subtropical	Wet	1321 ± 792	8.29 ± 11.29	264.2 ± 410.0	(Yao et al., 2007)
		Dry	1191 ± 825	4.90 ± 3.82	129.5 ± 197.2	
The Xijiang River (Mainstream)	Subtropical		2600		190.3–358.6	(Yao et al., 2007)
The Lower Meikong River	Tropical		1090 ± 290	6.24*	194.5	(Li et al., 2013)
The Yangtze River (Jinshui River) (headwater stream)	Subtropical		1147 ± 874	11.1 ± 4.5*	343 ± 413	(Luo et al., 2019)
		Dry	1562 ± 975		542 ± 477	
		Wet	834 ± 639		192 ± 278	
The upper Yangtze River (Daning river)	Subtropical		1198.2 ± 1122.9		329.8 ± 470.2	(Ni et al., 2019)
		Rainy	1243.7 ± 1111.5	8.1–14.1*	357.4 ± 483.7	
		Dry	1145.5 ± 1146.2	7.0–8.8*	288.7 ± 450.0	
The Zambezi River	Tropical	Wet	3102.5 **	0.05–1.51	350.75	(Teodoru et al., 2014)
		Dry	1150 **		51.92	
The Congo River	Tropical	High water	6001 ± 5008		1149 or 1520	(Borges et al., 2015a; Borges et al., 2015b)
		Low water	4867 ± 2578			
		Falling water	5321 ± 3383			
The Lower Red River	Tropical		1589 ± 43	12.22 ± 6.48	530.3 ± 16.9	(Le et al., 2018)
Caboolture River	Subtropical		3000 ± 33		379 ± 53	(Jeffrey et al., 2018)
Rajang River	Tropical	wet	2531 ± 188	0.55–2.93	141.67	(Müller-Dum et al., 2019)
		dry	2337 ± 304		125	
Lower Mississippi	Subtropical		1514 ± 652		172.8	(Reiman and Xu,

River					2019b)
<u>Amazonian Rivers</u>	<u>Tropical</u>	<u>259–7808</u>	<u>5.06</u>	<u>69.12–1321.92</u>	(Rasera et al., 2013)

530 * k values have been showed here because k_{600} values were not provided in references; ** the unit for μCO_2 is ppm.

The CO_2 fluxes in small rivers are similar to that in large rivers, which is contradictory to the finding in previous studies that CO_2 effluxes should be higher in small rivers ~~compared to~~ in large rivers due to the input of CO_2 -rich groundwater (Duvert et al., 2018). The depletion and diffusion effect may be responsible for the discrepancy (Johnson et al., 2007; Dinsmore et al., 2013). In the Dongjiang River Basin, groundwater could be easily diluted due to ample monsoon-induced precipitation, preventing it from supplying the small rivers with high concentrations of carbon dioxide. However, we recognize that the impact of groundwater on $p\text{CO}_2$ in small rivers may be overlooked in our sampling process since the CO_2 carried by groundwater can emit into the atmosphere within a very short distance (Duvert et al., 540 2018). In view of the above, it is recommended that further studies targeting the release of groundwater CO_2 to the atmosphere be carried out in the future.

5 Conclusion

Studying CO_2 emissions from subtropical rivers is an essential step toward more accurate estimates of global CO_2 evasion from river systems. By deploying floating chambers, seasonal changes in riverine $p\text{CO}_2$ and CO_2 evasion in the Dongjiang river catchment were investigated. Spatial and temporal patterns of $p\text{CO}_2$ were mainly affected by terrestrial carbon inputs and in-stream metabolism, both of which varied due to differential catchment settings, land cover, and hydrological conditions. Lateral soil CO_2 input and dilution effect caused by precipitation played critical roles in controlling riverine $p\text{CO}_2$ in small rivers, while the decomposition of allochthonous organic carbon is responsible for $p\text{CO}_2$ changes in large rivers as suggested by the ACO_2 - AO_2 stoichiometry line. k_{600} was higher in small rivers than large rivers and higher during the wet season than the dry season, both of which can be explained by the observed significant correlation between k_{600} and the flow velocity. In contrast to previous studies, similar CO_2 fluxes were observed among small and large rivers in the DJRB. It is suggested that the absence of commonly observed higher CO_2 fluxes in small rivers could be associated with the depletion effect 555 caused by abundant and persistent precipitation in this subtropical monsoon catchment. There is no doubt

that the spatial and temporal variation of CO₂ evasion in the DJRB reflected the complexity and diversity of controlling factors. As a step towards a more accurate estimate of the carbon budget in the catchment, comprehensive and systematic measurements of CO₂ evasion covering a broad range of stream sizes and seasons are of paramount importance.

560 *Data availability.* CO₂ emission data used in this study are available online at: <https://doi.org/10.25442/hku.13416281.v1> (Liu, 2020). Other data are available from the corresponding author Lishan Ran upon request at lsran@hku.hk.

565 *Author contributions.* BL and LR conceived the study. BL, MT, CC, XY, and LR carried out the fieldwork. BL, MT, and KS designed and performed the laboratory analysis. BL composed the manuscript with contributions from all authors.

Competing interests. The authors declare that they have no conflict of interest.

Acknowledgements. This work was financially supported by the Research Grants Council of Hong Kong (Grants: 17300619 and 27300118), the Hui Oi-Chow Trust Fund (Grant: 201801172006) and the National Natural Science Foundation of China (Grant: 41807318).

570

References

- Abril, G., Martinez, J. M., Artigas, L. F., Moreira-Turcq, P., Benedetti, M. F., Vidal, L., Meziane, T., Kim, J. H., Bernardes, M. C., Savoye, N., Deborde, J., Souza, E. L., Alberic, P., Landim de Souza, M. F., and Roland, F.: Amazon River carbon dioxide outgassing fuelled by wetlands, *Nature*, 505, 395-398, 575 <https://doi.org/10.1038/nature12797>, 2014.
- Abril, G., Bouillon, S., Darchambeau, F., Teodoru, C. R., Marwick, T. R., Tamooh, F., Ochieng Omengo, F., Geeraert, N., Deirmendjian, L., Polsenaere, P., and Borges, A. V.: Technical Note: Large overestimation of $p\text{CO}_2$ calculated from pH and alkalinity in acidic, organic-rich freshwaters, *Biogeosciences*, 12, 67-78, <https://doi.org/10.5194/bg-12-67-201510.5194>, 2015.
- 580 Alin, S. R., Rasera, M. d. F. F. L., Salimon, C. I., Richey, J. E., Holtgrieve, G. W., Krusche, A. V., and Snidvongs, A.: Physical controls on carbon dioxide transfer velocity and flux in low-gradient river systems and implications for regional carbon budgets, *Journal of Geophysical Research*, 116, G01009, <https://doi.org/10.1029/2010jg001398>, 2011.
- Almeida, R. M., Pacheco, F. S., Barros, N., Rosi, E., and Roland, F.: Extreme floods increase CO_2 585 outgassing from a large Amazonian river, *Limnology and Oceanography*, 62, 989-999, <https://doi.org/10.1002/lno.10480>, 2017.
- Amaral, J. H. F., Melack, J. M., Barbosa, P. M., MacIntyre, S., Kasper, D., Cortés, A., Silva, T. S. F., Nunes de Sousa, R., and Forsberg, B. R.: Carbon dioxide fluxes to the atmosphere from waters within flooded forests in the Amazon basin, *Journal of Geophysical Research: Biogeosciences*, 125, e2019JG005293, <https://doi.org/10.1029/2019JG005293>, 2020.
- 590 Battin, T. J., Luyssaert, S., Kaplan, L. A., Aufdenkampe, A. K., Richter, A., and Tranvik, L. J.: The boundless carbon cycle, *Nature Geoscience*, 2, 598-600, <https://doi.org/10.1038/ngeo618>, 2009.
- Borges, A. V., Delille, B., Schiettecatte, L. S., Gazeau, F., Abril, G., Frankignoulle, M. J. L., and 595 Oceanography: Gas transfer velocities of CO_2 in three European estuaries (Randers Fjord, Scheldt, and Thames), *Limnology Oceanography*, 49, 1630-1641, <https://doi.org/10.4319/lo.2004.49.5.1630>, 2004.
- Borges, A. V., Abril, G., Darchambeau, F., Teodoru, C. R., Deborde, J., Vidal, L. O., Lambert, T., and Bouillon, S.: Divergent biophysical controls of aquatic CO_2 and CH_4 in the World's two largest rivers, *Scientific Reports*, 5, 15614, 10.1038/srep15614, 2015a.
- Borges, A. V., Darchambeau, F., Teodoru, C. R., Marwick, T. R., Tamooh, F., Geeraert, N., Omengo, F. 600 O., Guérin, F., Lambert, T., Morana, C., Okuku, E., and Bouillon, S.: Globally significant greenhouse-gas emissions from African inland waters, *Nature Geoscience*, 8, 637-642, 10.1038/ngeo2486, 2015b.
- Borges, A. V., Darchambeau, F., Lambert, T., Bouillon, S., Morana, C., Brouyere, S., Hakoun, V., Jurado, A., Tseng, H. C., Descy, J. P., and Roland, F. A. E.: Effects of agricultural land use on fluvial carbon dioxide, methane and nitrous oxide concentrations in a large European river, the Meuse (Belgium), 605 *Science of The Total Environment*, 610-611, 342-355, <https://doi.org/10.1016/j.scitotenv.2017.08.047>, 2018.
- Chen, Q., Xu, W., Li, S., Fu, S., and Yan, J.: Aboveground biomass and corresponding carbon sequestration ability of four major forest types in south China, *Chinese Science Bulletin*, 58, 1551-1557, 10.1007/s11434-012-5100-8, 2013.
- 610 Chen, Y. D., Zhang, Q., Lu, X., Zhang, S., and Zhang, Z.: Precipitation variability (1956–2002) in the Dongjiang River (Zhujiang River basin, China) and associated large-scale circulation, *Quaternary International*, 244, 130-137, <https://doi.org/10.1016/j.quaint.2010.08.013>, 2011.
- Cole, J. J., Prairie, Y. T., Caraco, N. F., McDowell, W. H., Tranvik, L. J., Striegl, R. G., Duarte, C. M., Kortelainen, P., Downing, J. A., Middelburg, J. J., and Melack, J.: Plumbing the global carbon cycle: 615 Integrating inland waters into the terrestrial carbon budget, *Ecosystems*, 10, 172-185,

- <https://doi.org/10.1007/s10021-006-9013-8>, 2007.
- Denfeld, B. A., Frey, K. E., Sobczak, W. V., Mann, P. J., and Holmes, R. M.: Summer CO₂ evasion from streams and rivers in the Kolyma River basin, north-east Siberia, *Polar Research*, 32, 19704, <https://doi.org/10.3402/polar.v32i0.19704>, 2013.
- 620 Dickson, A. G., Sabine, C. L., and Christian, J. R.: Guide to best practices for ocean CO₂ measurements, North Pacific Marine Science Organization, 2007.
- Ding, J., Jiang, Y., Fu, L., Liu, Q., Peng, Q., and Kang, M.: Impacts of land use on surface water quality in a subtropical river basin: A case study of the Dongjiang River Basin, Southeastern China, *Water*, 7, 4427-4445, <https://doi.org/10.3390/w7084427>, 2015.
- 625 Dinsmore, K. J., Wallin, M. B., Johnson, M. S., Billett, M. F., Bishop, K., Pumpanen, J., and Ojala, A.: Contrasting CO₂ concentration discharge dynamics in headwater streams: A multi-catchment comparison, *Journal of Geophysical Research: Biogeosciences*, 118, 445-461, <https://doi.org/10.1002/jgrg.20047>, 2013.
- Drake, T. W., Raymond, P. A., and Spencer, R. G.: Terrestrial carbon inputs to inland waters: A current synthesis of estimates and uncertainty, *Limnology and Oceanography Letters*, 3, 132-142, <https://doi.org/10.1002/lol2.10055>, 2018.
- Duvert, C., Butman, D. E., Marx, A., Ribolzi, O., and Hutley, L. B.: CO₂ evasion along streams driven by groundwater inputs and geomorphic controls, *Nature Geoscience*, 11, 813-818, <https://doi.org/10.1038/s41561-018-0245-y>, 2018.
- 635 Fu, Y., Tang, C., Li, J., Zhao, Y., Zhong, W., and Zeng, X.: Sources and transport of organic carbon from the Dongjiang River to the Humen outlet of the Pearl River, southern China, *Journal of Geographical Sciences*, 24, 143-158, <https://doi.org/10.1007/s11442-014-1078-2>, 2014.
- Geeraert, N., Omengo, F. O., Borges, A. V., Govers, G., and Bouillon, S.: Shifts in the carbon dynamics in a tropical lowland river system (Tana River, Kenya) during flooded and non-flooded conditions, *Biogeochemistry*, 132, 141-163, <https://doi.org/10.1007/s10533-017-0292-2>, 2017.
- 640 Gómez-Gener, L., Rocher-Ros, G., Battin, T., Cohen, M. J., Dalmagro, H. J., Dinsmore, K. J., Drake, T. W., Duvert, C., Enrich-Prast, A., Horgby, Å., Johnson, M. S., Kirk, L., Machado-Silva, F., Marzolf, N. S., McDowell, M. J., McDowell, W. H., Miettinen, H., Ojala, A. K., Peter, H., Pumpanen, J., Ran, L., Riveros-Iregui, D. A., Santos, I. R., Six, J., Stanley, E. H., Wallin, M. B., White, S. A., and Sponseller, R. A.: Global carbon dioxide efflux from rivers enhanced by high nocturnal emissions, *Nature Geoscience*, 10.1038/s41561-021-00722-3, 2021.
- Guérin, F., Abril, G., Serça, D., Delon, C., Richard, S., Delmas, R., Tremblay, A., and Varfalvy, L.: Gas transfer velocities of CO₂ and CH₄ in a tropical reservoir and its river downstream, *Journal of Marine Systems*, 66, 161-172, <https://doi.org/10.1016/j.jmarsys.2006.03.019>, 2007.
- 650 Ho, D. T., Engel, V. C., Ferrón, S., Hickman, B., Choi, J., and Harvey, J. W.: On factors influencing air - water gas exchange in emergent wetlands, *Journal of Geophysical Research: Biogeosciences*, 123, 178-192, <https://doi.org/10.1002/2017JG004299>, 2018.
- Hope, D., Billett, M., and Cresser, M.: A review of the export of carbon in river water: fluxes and processes, *Environmental Pollution*, 84, 301-324, 1994.
- 655 Hope, D., Palmer, S. M., Billett, M. F., and Dawson, J. J. J. H. P.: Variations in dissolved CO₂ and CH₄ in a first - order stream and catchment: an investigation of soil-stream linkages, *Journal of Hydrological Processes*, 18, 3255-3275, <https://doi.org/10.1002/hyp.5657>, 2004.
- Hotchkiss, E., Hall Jr, R., Sponseller, R., Butman, D., Klaminder, J., Laudon, H., Rosvall, M., and Karlsson, J. J. N. G.: Sources of and processes controlling CO₂ emissions change with the size of streams and rivers, *Nature Geoscience*, 8, 696-699, <https://doi.org/10.1038/ngeo2507>, 2015.
- 660 Jeffrey, L. C., Santos, I. R., Tait, D. R., Makings, U., and Maher, D. T.: Seasonal drivers of carbon dioxide

- dynamics in a hydrologically modified subtropical tidal river and estuary (Caboolture River, Australia), *Journal of Geophysical Research: Biogeosciences*, 123, 1827-1849, <https://doi.org/10.1029/2017jg004023>, 2018.
- 665 Johnson, M. S., Weiler, M., Couto, E. G., Riha, S. J., and Lehmann, J.: Storm pulses of dissolved CO₂ in a forested headwater Amazonian stream explored using hydrograph separation, *Water resources research*, 43, <https://doi.org/10.1029/2007WR006359>, 2007.
- Johnson, M. S., Lehmann, J., Riha, S. J., Krusche, A. V., Richey, J. E., Ometto, J. P. H., and Couto, E. G.: CO₂ efflux from Amazonian headwater streams represents a significant fate for deep soil respiration, *Geophysical Research Letters*, 35, <https://doi.org/10.1029/2008GL034619>, 2008.
- 670 Kalbitz, K., and Kaiser, K.: Contribution of dissolved organic matter to carbon storage in forest mineral soils, *Journal of Plant Nutrition and Soil Science*, 171, 52-60, <https://doi.org/10.1002/jpln.200700043>, 2008.
- Lambert, T., Bouillon, S., Darchambeau, F., Morana, C., Roland, F. A. E., Descy, J.-P., and Borges, A. V.: Effects of human land use on the terrestrial and aquatic sources of fluvial organic matter in a temperate river basin (The Meuse River, Belgium), *Biogeochemistry*, 136, 191-211, 10.1007/s10533-017-0387-9, 2017.
- Lauerwald, R., Laruelle, G. G., Hartmann, J., Ciais, P., and Regnier, P. A.: Spatial patterns in CO₂ evasion from the global river network, *Global Biogeochemical Cycles*, 29, 534-554, <https://doi.org/10.1002/2014GB004941>, 2015.
- 680 Le Coz, J., Pierrefeu, G., and Paquier, A.: Evaluation of river discharges monitored by a fixed side-looking Doppler profiler, *Water Resources Research*, 44, <https://doi.org/10.1029/2008WR006967>, 2008.
- Le, T. P. Q., Marchand, C., Ho, C. T., Da Le, N., Duong, T. T., Lu, X., Doan, P. K., Nguyen, T. K., Nguyen, T. M. H., and Vu, D. A.: CO₂ partial pressure and CO₂ emission along the lower Red River (Vietnam), *Biogeosciences*, 15, 4799-4814, <https://doi.org/10.5194/bg-15-4799-2018>, 2018.
- 685 Li, S., Lu, X. X., and Bush, R. T.: CO₂ partial pressure and CO₂ emission in the Lower Mekong River, *Journal of Hydrology*, 504, 40-56, <https://doi.org/10.1016/j.jhydrol.2013.09.024>, 2013.
- Li, S., Ni, M., Mao, R., and Bush, R. T.: Riverine CO₂ supersaturation and outgassing in a subtropical monsoonal mountainous area (Three Gorges Reservoir Region) of China, *Journal of Hydrology*, 558, 460-469, <https://doi.org/10.1016/j.jhydrol.2018.01.057>, 2018.
- 690 Li, X., Xu, J., Shi, Z., and Li, R.: Response of Bacterial Metabolic Activity to the River Discharge in the Pearl River Estuary: Implication for CO₂ Degassing Fluxes, *Frontiers in Microbiology*, 10, 10.3389/fmicb.2019.01026, 2019.
- Liang, B., Hu, J. T., Li, S. Y., Ye, Y. X., Liu, D. H., and Huang, J.: Carbon system simulation in the Pearl River Estuary, China: Mass fluxes and transformations, *Journal of Geophysical Research: Biogeosciences*, 125, e2019JG005012, <https://doi.org/10.1029/2019jg005012>, 2020.
- 695 Luo, J., Li, S., Ni, M., and Zhang, J.: Large spatiotemporal shifts of CO₂ partial pressure and CO₂ degassing in a monsoonal headwater stream, *Journal of Hydrology*, 579, 124135, <https://doi.org/10.1016/j.jhydrol.2019.124135>, 2019.
- 700 Marx, A., Dusek, J., Jankovec, J., Sanda, M., Vogel, T., van Geldern, R., Hartmann, J., and Barth, J. A. C.: A review of CO₂ and associated carbon dynamics in headwater streams: A global perspective, *Reviews of Geophysics*, 55, 560-585, <https://doi.org/10.1002/2016rg000547>, 2017.
- Millero, F. J., Graham, T. B., Huang, F., Bustos-Serrano, H., and Pierrot, D.: Dissociation constants of carbonic acid in seawater as a function of salinity and temperature, *Marine Chemistry*, 100, 80-94, <https://doi.org/10.1016/j.marchem.2005.12.001>, 2006.
- 705 Moramarco, T., Saltalippi, C., and Singh, V. P.: Estimation of Mean Velocity in Natural Channels Based on Chiu's Velocity Distribution Equation, *Journal of Hydrologic Engineering*, 9, 42-50,

- doi:10.1061/(ASCE)1084-0699(2004)9:1(42), 2004.
- 710 Müller-Dum, D., Warneke, T., Rixen, T., Müller, M., Baum, A., Christodoulou, A., Oakes, J., Eyre, B. D.,
and Notholt, J.: Impact of peatlands on carbon dioxide (CO₂) emissions from the Rajang River and
Estuary, Malaysia, *Biogeosciences*, 16, 17-32, <https://doi.org/10.5194/bg-16-17-2019>, 2019.
- Ni, M., Li, S., Luo, J., and Lu, X.: CO₂ partial pressure and CO₂ degassing in the Daning River of the
upper Yangtze River, China, *Journal of Hydrology*, 569, 483-494,
<https://doi.org/10.1016/j.jhydrol.2018.12.017>, 2019.
- 715 Ran, L., Lu, X. X., Yang, H., Li, L., Yu, R., Sun, H., and Han, J.: CO₂ outgassing from the Yellow River
network and its implications for riverine carbon cycle, *Journal of Geophysical Research: Biogeosciences*,
120, 1334-1347, <https://doi.org/10.1002/2015jg002982>, 2015.
- Ran, L., Li, L., Tian, M., Yang, X., Yu, R., Zhao, J., Wang, L., and Lu, X.: Riverine CO₂ emissions in the
Wuding River catchment on the Loess Plateau: Environmental controls and dam impoundment impact,
720 *Journal of Geophysical Research: Biogeosciences*, 122, 1439-1455,
<https://doi.org/10.1002/2016JG003713>, 2017a.
- Ran, L., Lu, X. X., and Liu, S.: Dynamics of riverine CO₂ in the Yangtze River fluvial network and their
implications for carbon evasion, *Biogeosciences*, 14, 2183-2198, <https://doi.org/10.5194/bg-14-2183-2017>, 2017b.
- 725 Ran, L., Lu, X., Fang, N., and Yang, X.: Effective soil erosion control represents a significant net carbon
sequestration, *Scientific reports*, 8, 12018, 2018.
- Ran, Y., Li, X., Lu, L., and Li, Z.: Large-scale land cover mapping with the integration of multi-source
information based on the Dempster-Shafer theory, *International Journal of Geographical Information
Science*, 26, 169-191, 2012.
- 730 Rasera, M. d. F. F., Krusche, A. V., Richey, J. E., Ballester, M. V., and Victoria, R. L.: Spatial and temporal
variability of pCO₂ and CO₂ efflux in seven Amazonian Rivers, *Biogeochemistry*, 116, 241-259,
<https://doi.org/10.1007/s10533-013-9854-0>, 2013.
- Raymond, P. A., Zappa, C. J., Butman, D., Bott, T. L., Potter, J., Mulholland, P., Laursen, A. E.,
McDowell, W. H., and Newbold, D.: Scaling the gas transfer velocity and hydraulic geometry in streams
735 and small rivers, *Limnology and Oceanography: Fluids and Environments*, 2, 41-53,
<https://doi.org/10.1215/21573689-1597669>, 2012.
- Raymond, P. A., Hartmann, J., Lauerwald, R., Sobek, S., McDonald, C., Hoover, M., Butman, D., Striegl,
R., Mayorga, E., and Humborg, C.: Global carbon dioxide emissions from inland waters, *Nature*, 503,
355-359, <https://doi.org/10.1038/nature12760>, 2013.
- 740 Reiman, J. H., and Xu, Y. J.: Diel Variability of pCO₂ and CO₂ Outgassing from the Lower Mississippi
River: Implications for Riverine CO₂ Outgassing Estimation, *Water*, 11, 43, 2019a.
- Reiman, J. H., and Xu, Y. J.: Dissolved carbon export and CO₂ outgassing from the lower Mississippi
River – Implications of future river carbon fluxes, *Journal of Hydrology*, 578, 124093,
<https://doi.org/10.1016/j.jhydrol.2019.124093>, 2019b.
- 745 Sawakuchi, H. O., Neu, V., Ward, N. D., Barros, M. d. L. C., Valerio, A. M., Gagne-Maynard, W., Cunha,
A. C., Less, D. F. S., Diniz, J. E. M., Brito, D. C., Krusche, A. V., and Richey, J. E.: Carbon dioxide
emissions along the lower Amazon River, *Frontiers in Marine Science*, 4,
<https://doi.org/10.3389/fmars.2017.00076>, 2017.
- 750 Stets, E. G., Butman, D., McDonald, C. P., Stackpoole, S. M., DeGrandpre, M. D., and Striegl, R. G.:
Carbonate buffering and metabolic controls on carbon dioxide in rivers, *Global Biogeochemical Cycles*,
31, 663-677, <https://doi.org/10.1002/2016gb005578>, 2017.
- Tao, Z., Gao, Q., Wang, Z., Zhang, S., Xie, C., Lin, P., Ruan, X., Li, S., and Mao, H.: Estimation of
carbon sinks in chemical weathering in a humid subtropical mountainous basin, *Chinese Science Bulletin*,

- 56, 3774-3782, <https://doi.org/10.1007/s11434-010-4318-6>, 2011.
- 755 Teodoru, C., Nyoni, F., Borges, A., Darchambeau, F., Nyambe, I., and Bouillon, S.: Spatial variability and temporal dynamics of greenhouse gas (CO₂, CH₄, N₂O) concentrations and fluxes along the Zambezi River mainstem and major tributaries, *Biogeosciences Discussion*, 11, 16391-16445, <https://doi.org/10.5194/bgd-11-16391-2014>, 2014.
- 760 Tian, M., Yang, X., Ran, L., Su, Y., Li, L., Yu, R., Hu, H., and Lu, X. X.: Impact of land cover types on riverine CO₂ outgassing in the Yellow River source region, *Water*, 11, 2243, <https://doi.org/10.3390/w11112243>, 2019.
- Wanninkhof, R.: Relationship between wind speed and gas exchange over the ocean, *Journal of Geophysical Research: Oceans*, 97, 7373-7382, <https://doi.org/10.1029/92JC00188>, 1992.
- 765 Weiss, R. F.: Carbon dioxide in water and seawater: the solubility of a non-ideal gas, *Marine Chemistry*, 2, 203-215, [https://doi.org/10.1016/0304-4203\(74\)90015-2](https://doi.org/10.1016/0304-4203(74)90015-2), 1974.
- Xuan, Y., Cao, Y., Tang, C., and Li, M.: Changes in dissolved inorganic carbon in river water due to urbanization revealed by hydrochemistry and carbon isotope in the Pearl River Delta, China, *Environmental Science and Pollution Research*, 10.1007/s11356-020-08454-4, 2020.
- 770 Yao, G., Gao, Q., Wang, Z., Huang, X., He, T., Zhang, Y., Jiao, S., and Ding, J.: Dynamics of CO₂ partial pressure and CO₂ outgassing in the lower reaches of the Xijiang River, a subtropical monsoon river in China, *Science of The Total Environment*, 376, 255-266, <https://doi.org/10.1016/j.scitotenv.2007.01.080>, 2007.
- Zhang, L., Qin, X., Liu, P., Huang, Q., Lan, F., and Ji, H.: Estimation of carbon sink fluxes in the Pearl River basin (China) based on a water-rock-gas-organism interaction model, *Environmental Earth Sciences*, 74, 945-952, <https://doi.org/10.1007/s12665-014-3788-2>, 2015.
- 775 Zhang, S., Lu, X. X., Higgitt, D. L., Chen, C.-T. A., Han, J., and Sun, H.: Recent changes of water discharge and sediment load in the Zhujiang (Pearl River) Basin, China, *Global and Planetary Change*, 60, 365-380, <https://doi.org/10.1016/j.gloplacha.2007.04.003>, 2008.
- Zhang, T., Li, J., Pu, J., and Yuan, D.: Carbon dioxide exchanges and their controlling factors in Guijiang River, SW China, *Journal of Hydrology*, 578, 124073, <https://doi.org/10.1016/j.jhydrol.2019.124073>, 2019.
- 780 Zhang, W., Li, H., Xiao, Q., and Li, X.: Urban rivers are hotspots of riverine greenhouse gas (N₂O, CH₄, CO₂) emissions in the mixed-landscape chaohu lake basin, *Water Research*, 189, 116624, <https://doi.org/10.1016/j.watres.2020.116624>, 2021.
- 785